

## ISO observations of Wolf-Rayet galaxy Haro 3<sup>★</sup>

L. Metcalfe<sup>1</sup>, S. J. Steel<sup>3</sup>, P. Barr<sup>1</sup>, J. Clavel<sup>1</sup>, M. Delaney<sup>3</sup>, P. Gallais<sup>1,2</sup>, R. J. Laureijs<sup>1</sup>, K. Leech<sup>1</sup>, B. McBreen<sup>3</sup>, S. Ott<sup>1</sup>, N. Smith<sup>4</sup>, and L. Hanlon<sup>3</sup>

<sup>1</sup> ISO Science Operations Centre, Astrophysics Division of ESA, Villafranca, Spain

<sup>2</sup> CEA, DSM/DAPNIA, CE-Saclay, F-91191 Gif-sur-Yvette Cedex, France

<sup>3</sup> Physics Department, University College, Belfield, Dublin 4, Ireland

<sup>4</sup> Regional Technical College, Rossa Ave., Cork, Ireland

Received 16 July 196 / Accepted 13 August 1996

**Abstract.** Observations of the blue compact dwarf galaxy Haro 3 have been obtained with the ISOCAM and ISOPHOT instruments on the Infrared Space Observatory (ISO). The PHT-S spectrum (6–12  $\mu\text{m}$ ) is dominated by four emission bands that are frequently attributed to polycyclic aromatic hydrocarbons (PAHs) and strong SIV emission. Two CAM filters, LW6 (7–8.5  $\mu\text{m}$ ) and LW3 (12–18  $\mu\text{m}$ ) were used to map the galaxy. The LW6 image is essentially a map of the galaxy in the 7.7  $\mu\text{m}$  PAH feature. The emission in both maps is extended and matches very well a map of the H $\alpha$  emission. Both maps show coincident single peak emission and a spatial correspondance with the nuclear region of the galaxy and the brightest optical region, an off-axis starburst containing Wolf-Rayet stars. A ratio map of LW6/LW3 images shows two peaks on a ridge elongated along the optical axis of the galaxy.

**Key words:** infrared: galaxies: individual: Haro 3 – galaxies: starburst – ISM: molecules – ISM: dust

### 1. Introduction

Blue compact dwarf galaxies (BCD) are characterised by their small size ( $\leq 5$  kpc diameter), low metallicity, ultraviolet excess and spectra dominated by narrow emission lines. BCDs have been the subject of intense scrutiny over recent years, as they form excellent laboratories for the study of galaxy formation and evolution (see for example Kunth et al. 1994). Haro 3 (Mkn 35, NGC 3353) is a BCD dominated in the optical by several starburst regions (Fig. 1). Age estimates for the starbursts indicate that the current phase of violent star formation was initiated within the last 5 million years (Steel et al. 1996a). The

*Send offprint requests to:* lmetcalf@iso.vilspa.esa.es

<sup>★</sup> ISO is an ESA project with instruments funded by ESA Member States (especially the PI countries: France, Germany, the Netherlands and the United Kingdom) and with the participation of ISAS and NASA.

starburst with highest surface brightness (Region A, Fig. 1) is also the youngest star forming region in the galaxy at 1.5 to 3 Myr, and is characterised by the presence of more than 150 Wolf-Rayet stars (Steel et al. 1996b). Hence Haro 3 can be classified as a Wolf-Rayet galaxy (Conti 1991).

Haro 3 was observed by IRAS, and has a far infrared to blue luminosity ratio  $L_{FIR}/L_B$  of 2.2 (Belfort et al. 1987) which is a typical value for BCDs. The value of  $L_{FIR}/L_B$  is significantly lower than that found in disturbed spirals and IRAS galaxies which also have enhanced star formation. A value of  $H_o = 75 \text{ kms}^{-1} \text{ Mpc}^{-1}$  is assumed. A mass of  $1.2 \times 10^9 M_\odot$  for Haro 3 is reported in Thuan and Martin 1981.

### 2. Observations and Data Reduction

The observations reported here were obtained using the mid-infrared camera ISOCAM (Cesarsky et al. 1996) and the photometric mode of the ISO photopolarimeter ISOPHOT (Lemke et al. 1996) on the Infrared Space Observatory (ISO) (Kessler et al. 1996).

The CAM images were obtained by making  $4 \times 4$  rasters with the CAM 6'' per pixel f.o.v. and a step size of 96'' (16 pixels). The LW6 raster began with 29 stabilisation readouts and the LW3 raster with 9. Initial raster steps allow the transient background signal to stabilise, before the target appears on the detector array (and introduces its own transient). About eighteen 5.04 second integrations were obtained at each raster position. The total observation time for both filters was about 3800 seconds.

The data was reduced using the CAM Interactive Analysis S/W (CIA)<sup>1</sup>. Reduction began from the Pipeline (OLP) products CIER and IIPH (Siebenmorgen et al. 1996). The data was organised into data cubes for each filter. It was found that optimum deglitching of images was achieved by applying a CIA multiresolution median transform method (Starck et al. 1995).

<sup>1</sup> CIA is a joint development by the ESA Astrophysics Division and the ISOCAM Consortium led by the ISOCAM PI, C. Cesarsky, Direction des Sciences de la Matière, CEA, France.

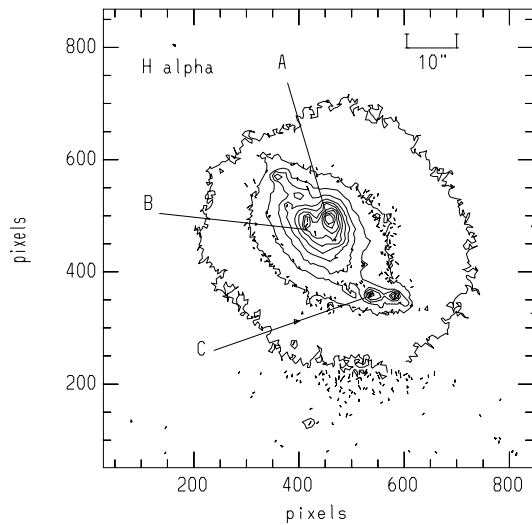


**Fig. 1.** Logarithmic contour map of Haro 3 ( $\alpha_{2000} = 10^h 45^m 22.7^s$ ,  $\delta_{2000} = +55^d 57' 35.9''$ ) in H $\alpha$  light (Steel et al. 1996b). The brightest optical star forming regions are labelled A, B and C respectively. Dimensions are  $1.5' \times 1.5'$ . North is up and east to the left.

Seriously unstabilised frames were masked out from the final processing so that only frames stabilised to within about 10% of the final signal level for each detection were used. The success of deglitching and of transient rejection was verified by inspection of the time history of the array pixels through the data cubes. Generally, careful usage of the existing deglitching S/W will remove most glitches, but care has to be taken that portions of useful signal are not also removed. Manual masking of anomalous data can complement automatic deglitching routines. The signal-free column (24) of the detector was masked out manually.

The data cubes were assembled into raster images in each filter using a CIA routine which generates a flat-field from the median of all the frames in the cube. The various pointings of the raster scan are merged into a single image of the target field scaled to  $\text{ADU s}^{-1}$  per unit electronic gain. The image so derived was then scaled to units of  $\text{mJy arcsec}^{-2}$  using the photometric scaling factors to be issued in the August 1996 release of CAM Calibration files, which also are the values quoted in Cesarsky et al. 1996 (in this issue). This calibration is referred to a source of constant  $\nu I(\nu)$  and the fluxes quoted in this paper for filter measurements assume such a source spectrum. The fact that the galaxy spectrum clearly deviates from this in the PHT-S range will nonetheless contribute negligibly to the CAM LW6 measurement, because the actual spectral shape is highly symmetrical in the LW6 bandpass.

The PHT-S spectrum has been obtained by measuring the difference signal in a  $25'' \times 25''$  aperture centred on the peak of the LW6 emission and two background positions outside the galaxy using the ISOPHOT focal plane chopper. The calibration of the spectrum was performed by using a PHT-S spectral response function derived from two calibration stars. The relative

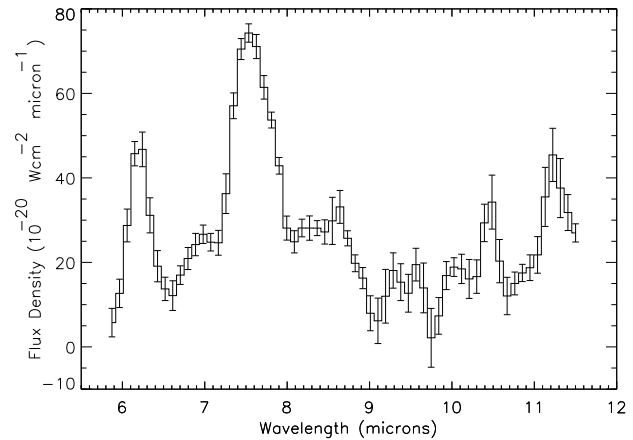


**Fig. 2.** PHT-S spectrum of Haro 3, centred on the brightest CAM pixel.

photometric uncertainty of the PHT-S spectrum is of order 20% when comparing different parts of the spectrum that are more than a few microns apart. The absolute photometric uncertainty is of order 30% for bright calibration sources. To improve the signal-to-noise ratio we have Hanning smoothed the spectrum.

### 3. Results and Discussion

An important source of infrared flux, and a significant contributor in the 3 to 20  $\mu\text{m}$  region, comes from radiation attributed to the presence of polycyclic aromatic hydrocarbons (PAHs), formed in the atmospheres of carbon-rich cool stars and molecular clouds (Puget and Léger 1989). Identification of specific PAH emission lines comes from comparison with laboratory spectroscopic data (Allamandola et al. 1989; Puget and Léger 1989).

The PHT-S spectrum for the long wavelength array is presented in Fig. 2. Most striking is the presence of the family of unidentified infrared emission bands at 6.2, 7.7, 8.6, and 11.3  $\mu\text{m}$  generally attributed to emission from PAHs (e.g. Léger et al. 1989). Another prominent feature in the spectrum is the SIV line at 10.5  $\mu\text{m}$ . We notice that the features appear to be situated on a continuum in the 7-11.5  $\mu\text{m}$  range of about  $15 \times 10^{-20} \text{ W cm}^{-2} \mu\text{m}^{-1}$  with a depression in the 9-11  $\mu\text{m}$  range where silicate absorption could be present. The pedestal emission between 7 and 9  $\mu\text{m}$  could be caused by a blending of other PAH features (Léger et al. 1989) but we cannot rule out the presence of ionic line emission such as [ArII].

To quantify the emission properties in the main features we have listed intensities in Table 1 assuming that the bands are situated on a local continuum. From Table 1 we derive ratios of  $I_{\lambda}(6.2\mu\text{m})/I_{\lambda}(7.7\mu\text{m}) = 0.67 \pm 0.15$  and  $I_{\lambda}(11.3\mu\text{m})/I_{\lambda}(7.7\mu\text{m}) = 0.41 \pm 0.10$ . The ratio  $I_{\lambda}(6.2\mu\text{m})/I_{\lambda}(7.7\mu\text{m})$  is typical of what has been found in reflection nebulae and HII regions (Cohen et al. 1989). The ratio  $I_{\lambda}(11.3\mu\text{m})/I_{\lambda}(7.7\mu\text{m})$  is on the high end of the ratios seen in galactic objects (usually 0.2 to 0.3) and might indicate that the PAHs emitting in Haro 3 have a high fraction of C-H solo bonds in comparison with C=C bonds which should give rise to the 7.7  $\mu\text{m}$  emission. However the aperture size of

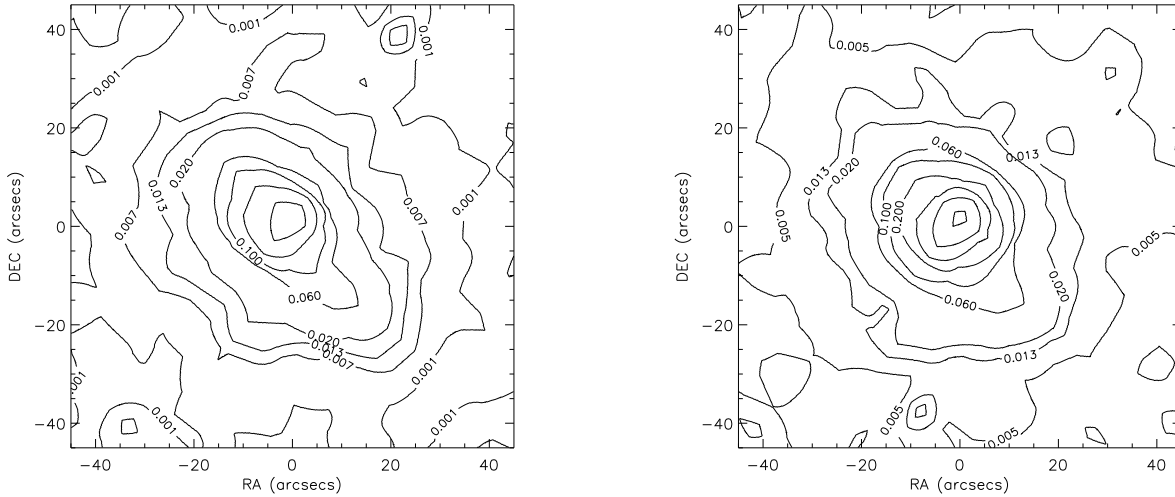


**Fig. 3.** Contour maps of Haro 3 using (a) the LW6 filter and (b) the LW3 filter. Both maps are of dimensions  $1.5' \times 1.5'$ , orientated North up and East left. The reference pixel, (0, 0) is centred on the  $H\alpha$  map (Fig. 1). The contour unit is  $\text{mJy arcsec}^{-2}$ .

**Table 1.** Features in the PHT-S spectrum. The fourth column gives the best estimate of the continuum flux at the centre wavelength of the feature.

line ID	$\lambda$ $\mu\text{m}$	$I_\lambda$ $10^{-20} \text{ W cm}^{-2}$	continuum $10^{-20} \text{ W cm}^{-2} \mu\text{m}^{-1}$
PAH 6.2	6.24	$18 \pm 1$	4
PAH 7.7	7.53	$27 \pm 6$	23
PAH 8.6	8.64	$2.2 \pm 0.4$	21
PAH 11.3	11.3	$11 \pm 1$	19
SIV	10.5	$5.2 \pm 1.0$	11

$25''$  corresponds to 1.6 kpc, so the spectrum is a summation of the central region of Haro 3 including the major starburst regions. It is also important to determine if the SIV emission is a characteristic of BCDs and if it has any connection with the Wolf-Rayet system and gas density. Further observations of similar systems should clarify this issue.

The photometric maps of Haro 3 are presented in Fig. 3. The LW6 map is dominated by the  $7.7 \mu\text{m}$  PAH feature whereas the LW3 map contains contributions from warm dust, nebular line emission including NeII and other PAH features (Moutou et al. 1996). Further investigations, possibly using the Circular Variable Filter (CVF) on ISOCAM, are needed to determine the relative contribution of these sources to the LW3 emission. The peaks in both the LW6 and LW3 maps (Fig. 3) are coincident with each other and also consistent with the two major regions of star formation at the centre of Haro 3 (Regions A and B in Fig. 1). Region B consists of 3-4 star forming knots which lie to the south-east of the dominant optical feature Region A, the youngest starburst and location of the Wolf-Rayet population. The remarkable feature is the similar overall shape and extent of both maps. Furthermore both maps are also similar in extent to the  $H\alpha$  map (Fig. 1) with the two big spurs of emission ex-

tending to the northeast and southwest where the latter spur is coincident with star forming region C.

The LW6 map is dominated by the  $7.7 \mu\text{m}$  PAH feature and hence the PAHs exist throughout the galaxy and are at least as extensive as the  $H\alpha$  emission. The LW3 map is remarkable in its similarity to the LW6 map and hence it is probable that the  $12\text{--}18 \mu\text{m}$  emission contains a significant contribution from PAH emission. The total flux density in LW3 is  $300 \pm 70 \text{ mJy}$  and is reasonably consistent with the  $210 \text{ mJy}$  in the IRAS  $12 \mu\text{m}$  band especially because the filter bandwidths are not identical. In the LW6 map the total emission is  $149 \pm 30 \text{ mJy}$  which is approximately twice the value obtained for the  $7.7 \mu\text{m}$  feature from the PHT-S spectrum (Table 1). The larger value is expected because of the limited aperture of PHT-S and also because a continuum had been removed from the PHT-S spectrum. The total luminosity in the four PAH features listed in Table 1 is  $3 \times 10^6 L_\odot$  assuming a distance 13.1 Mpc. This value should be increased by a factor of about 2 to account for the extended emission outside the PHT-S aperture. The ratio of the emission in the PAH features is  $4 \times 10^{-3}$  of the total far-infrared luminosity of  $1.6 \times 10^9 L_\odot$ . We expect this ratio to increase significantly when the contribution of PAH's to the emission in the LW3 map is determined.

The ratio map LW6/LW3 is presented in Fig. 4. The contours range from a ratio value of 0.15 to 0.64. The fainter contours lie at the outer regions of the galaxy and at the limit of the background, below which values are unreliable. The stronger contours reveal two peaks, similar to those of the optical (see Fig. 1), joined by a ridge extending northeast to southwest. The northeast peak is about coincident with star forming regions A and B and the southwest peak coincides with star forming region C. The drop in the ratio at the centre of the map separating the two peaks may be caused by a decrease in PAH emission in the LW3 bandpass relative to the  $7.7 \mu\text{m}$  emission in the LW6 bandpass in the vicinity of optically bright regions A and B,

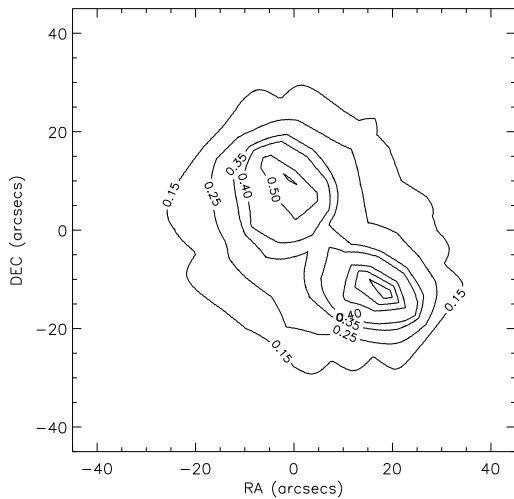


**Fig. 4.** Ratio map of LW6/LW3. Dimensions are  $1.5' \times 1.5'$  and orientation is North up and East left. The reference pixel, (0, 0) is centred on the H $\alpha$  map (Fig. 1).

and of the fainter HII region C. In a galactic environment most molecules will be susceptible to ionization and dehydrogenation. PAH molecules are susceptible to dissociation by strong UV radiation fields such as those encountered near OB associations with small PAHs surviving only a few years (Allain et al. 1996). Consequently, a reduction in PAH emission may be occurring near starburst regions A/B, and C. This phenomenon is supported by observations of a decrease in the ratio of  $12 \mu\text{m}$  to total far-infrared flux for giant HII regions and starburst galaxies (Gosh et al. 1986).

#### 4. Conclusions

ISO observations of the BCD Wolf-Rayet galaxy Haro 3 have been made with the CAM and PHT instruments. The PHT-S spectrum from the central  $25'' \times 25''$  is dominated by four PAH features and strong SIV emission. ISOCAM mapped the galaxy in the LW6 and LW3 wavebands. Both wavebands have coincident single peak maxima coinciding with the nuclear region of the galaxy and the major optical starburst with a Wolf-Rayet stellar population. The LW6 and LW3 maps are extended and approximately match the H $\alpha$  map of the galaxy. A ratio map of LW6/LW3 is elongated along the major optical axis of the galaxy, and exhibits a drop near the centre of the ridge. A possible interpretation of this result is the weakening of the LW3 flux by the intense radiation field of the central starbursts. Further observations are needed at higher spatial resolution and at larger wavelength coverage to determine the positional relationship between the optical starbursts and peak infrared emission, and the relative contribution to the LW3 flux of dust, PAH and nebular line emission.

#### References

Allain T., Leach S., Sedlmayr E., 1996, A&A 305, 602.

- Allamandola L. J., Bregman J. D., Sandford S. A., et al. 1989, ApJ 345, L59.
- Belfort P., Mochkovitch R., Dennefeld M., 1987, A&A 176, 1.
- Cesarsky C.J. et al. 1996, A&A (this issue).
- Cohen M., Tielens A.G.G.M., & Bregman J., et al. 1989, ApJ 341, 246.
- Conti P. S., 1991, ApJ 377, 115.
- Moutou C., Léger A., d'Hendecourt L., 1996, A&A 310, 297.
- Gosh S. K., Drapatz S., Peppel U. C., 1986, A&A 167, 341.
- Kessler M. et al. 1996, A&A (this issue).
- Kunth D., Lequeux J., Sargent W. L. W., Viallefond F., 1994, A&A 282, 709.
- Laureijs R. J., Richards P. J., Krüger, 1996, ISOPHOT Data User's Manual v.2.0, SAI/95-220/Doc.
- Léger A., d'Hendecourt L., & Défourneau D., 1989, A&A 216, 148.
- Lemke D. et al. 1996, A&A (this issue).
- Puget J. L., Léger A., 1989, Ann. Rev. Astron. Astrophys. 27, 161.
- Siebenmorgen R., Starck J.L., Cesarsky D., Guest, S. and Sauvage M., ISOCAM Data User's Manual V.2.1, ESA Document, Reference SAI/95-221/DC, 1996.
- Starck J.L., Bijaoui A., Murtagh F., 1995, Graphical Models and Image Processing, Vol. 57, 5, p420.
- Steel S. J., Smith N., Metcalfe L., Rabbette M., McBreen B., 1996a, A&A 311, 721.
- Steel S. J., Prada F., Perez E., McBreen B., Rabbette M., Metcalfe L., Smith N., 1996b (in preparation).
- Thuan T. X., Martin G. E., 1981, ApJ 247, 823.